JBC RESEARCH ARTICLE

Complex G-protein signaling of the adhesion GPCR, ADGRA3

Received for publication, March 5, 2025 Published, Papers in Press, March 22, 2025,
https://doi.org/10.1016/j.jbc.2025.108441

Sofie M. Bagger[1], Hannes Schihada[2], Anna L. S. Walser[1], Anna K. Drzazga[1], Lukas Grätz[2], Tiago Palmisano[3,4], Christina K. Kuhn[5], Maša Mavri[1], Ann-Sophie Mølleskov-Jensen[1], Gregory G. Tall[6], Torsten Schöneberg[5], Signe J. Mathiasen[1,3,4], Jonathan A. Javitch[3,4], Gunnar Schulte[2], Katja Spiess[1], and Mette M. Rosenkilde[1,*]

From the [1]Department of Biomedical Sciences, Faculty of Health and Medical Sciences, University of Copenhagen, Copenhagen, Denmark; [2]Department of Physiology and Pharmacology, Section of Receptor Biology and Signaling, Karolinska Institutet, Stockholm, Sweden; [3]Departments of Psychiatry and Molecular Pharmacology and Therapeutics, Columbia University Vagelos College of Physicians and Surgeons, New York, New York, USA; [4]Division of Molecular Therapeutics, New York State Psychiatric Institute, New York, New York, USA; [5]Molecular Biochemistry, Medical Faculty, Rudolf Schönheimer Institute of Biochemistry, Leipzig, Germany; [6]Department of Pharmacology, University of Michigan School of Medicine, Ann Arbor, Michigan, USA

Reviewed by members of the JBC Editorial Board. Edited by Henrik Dohlman

ADGRA3 (GPR125) is an orphan adhesion G protein–coupled receptor (aGPCR) involved in planar cell polarity, primarily through recruitment of the signaling components disheveled (DVL) during vertebrate gastrulation and discs large homolog 1, implicated in cancer. Limited knowledge exists of the canonical G protein–coupled receptor pathways downstream of ADGRA3. Here, we employed a series of human cell line–based signaling assays to gain insight into the G protein–mediated signaling of ADGRA3. We designed ADGRA3 constructs based on transcript variant analysis in publicly available human liver and brain RNA-seq datasets. Cleavage in the GPCR autoproteolysis site (GPS) is an aGPCR hallmark; thus, we generated a truncated ADGRA3 (C-terminal fragment, CTF) corresponding to a potential cleavage at the GPS. We found low-level activation of Gi and Gs by ADGRA3 and slightly more by its CTF. As the N terminus of the CTF constitutes a class-defined tethered agonist (so-called stachel peptide), we removed the initial three amino acids of the CTF. This resulted in abrogated G protein–mediated signaling, as observed for other aGPCRs. Due to the central role of ADGRA3 in planar cell polarity signaling through DVL recruitment, we investigated the G-protein signaling in the absence of DVL1-3 and found it sustained. No transcriptional activation was observed in an assay of downstream β-catenin activity. Collectively, this establishes classical G protein–mediated signaling for ADGRA3.

Adhesion G protein–coupled receptors (aGPCRs) constitute class B2 of the superfamily of G protein–coupled receptors (GPCRs). As a distinct class of receptors, aGPCRs regulate processes in various physiological systems, including the nervous and musculoskeletal systems, and play curtail roles in metabolism, immunity, and development (1). Mutations and dysregulation of aGPCRs in humans are associated with diverse diseases, including developmental defects, neurological disorders, and cancer (1). Signal transduction from aGPCRs spans coupling to heterotrimeric G proteins and diverse alternative pathways, including β-arrestin recruitment and β-catenin–mediated signaling engagement (2, 3). aGPCRs are divided into nine families based on their phylogenetic relations, of which family III comprises ADGRA3 (previously known as GPR125) in addition to ADGRA2 (GPR124) and ADGRA1 (GPR123) (4, 5). ADGRA1-3 are all expressed in the brain and linked to developmental signaling pathways (6–12). Furthermore, ADGRA3 expression is associated with various cancers showing both oncogenic and tumor-suppressive effects (13–16).

ADGRA3 was initially identified as a spermatogonial stem cell marker (17), and the knockdown of ADGRA3 in male mice leads to obstructive azoospermia with high penetrance (18), while female mice lacking ADGRA3 develop a closed vagina to a similar extent (12). In mammary progenitors, ADGRA3 expression congregates at ductal tips during morphogenesis, and high expression predicts early tumor onset and poor outcome (13). In lacrimal gland progenitors, its expression segregates to the tip of migrating embryonic lacrimal ducts, and its absence leads to dry eyes and blepharitis (19). Further, ADGRA3 plays a role in adipose thermogenesis as overexpression or activation-induced expression stimulates browning of adipocytes (20). At the cellular level, ADGRA3 contributes to planar cell polarity (PCP) regulation of the zebrafish embryo through redistribution of the scaffolding phosphoprotein disheveled (DVL) (11, 21). ADGRA3 also interacts with the scaffolding protein discs large homolog 1 (Dlg1) through its C-terminal ETTV domain (Glu^{1318}-Thr^{1319}-Thr^{1320}-Val^{1321}) (21–23). Moreover, the knockdown of ADGRA3 in osteoclasts downregulates receptor activator of nuclear factor kappa-B ligand–induced pathways, which are important for osteoclastogenesis (24).

aGPCRs contain large extracellular N termini harboring several adhesive domains and the conserved GPCR autoproteolysis-inducing domain comprising a GPCR proteolytic site (GPS) motif. The GPS in most ADGRA3 vertebrate orthologs is SL|S/G (where | denotes the potential cleavage point). Although this differs from the canonical GPS motif

* For correspondence: Mette M. Rosenkilde, rosenkilde@sund.ku.dk.

(HL|S/T), autoproteolytic cleavage of ADGRA3 was suggested based on immunoblot fragment sizes, yet the precise location of the cleavage site was not ascertained (21). In general, upon aGPCR autoproteolysis, the fragments remain noncovalently associated as a heterodimer: an extracellular N-terminal fragment (NTF) and a C-terminal fragment (CTF) with the heptahelical transmembrane GPCR fold (Fig. 1*A*) (25, 26). As a general concept, removing the NTF at the GPS results in enhanced CTF signaling relative to the full-length (FL) receptor, suggesting a suppressive activity of the NTF among aGPCRs (27). Furthermore, evidence is building towards a role of the class-defined so-called *stachel* peptide immediately downstream of the GPS to work as an intramolecular tethered agonist on aGPCRs, internally controlling receptor activity (28–31). Moreover, alternative splicing events and multiple transcript variants are reported for several aGPCR class members, some with tissue-specific expression, implying that caution should be taken when designing and evaluating ectopic (over)expression studies (32, 33).

Here, we probe the downstream signaling of ADGRA3 through heterotrimeric G proteins. First, we analyzed the transcript variants of ADGRA3 in publicly available human liver and brain RNA-seq datasets, which guided the design of ADGRA3 constructs employed in this study. Next, we generated a truncated ADGRA3 construct where the NTF was removed, corresponding to the functional cleavage of the receptor at the GPS site, to investigate the ability of ADGRA3 and its potential CTF to initiate signaling through heterotrimeric G proteins (Fig. 1, *A* and *B*). ADGRA3 interacts physically with $G\alpha_i$, but so far, this has not been verified functionally (21). Therefore, we systematically studied ADGRA3-mediated G-protein activation. Due to the previously established interaction with DVLs (11, 21), we used cells with and without DVLs (ΔDVL1-3) (34) to probe G-protein signaling dependency on the presence of DVL. Lastly, we investigated the effect of truncating the putative intramolecular "tethered" agonist within the ADGRA3 CTF. Taken together, our data shed light on G protein–mediated signaling by ADGRA3, which is hitherto unreported for class III aGPCRs.

Results

One dominant transcript variant of ADGRA3 is expressed in the human liver and brain

The genomic architecture of aGPCRs is often complex, each coding sequence stretching over numerous exons, allowing alternative splicing events that produce multiple transcript variants (32, 35). Since the various transcript variants from an aGPCR gene can exhibit significantly different functions and

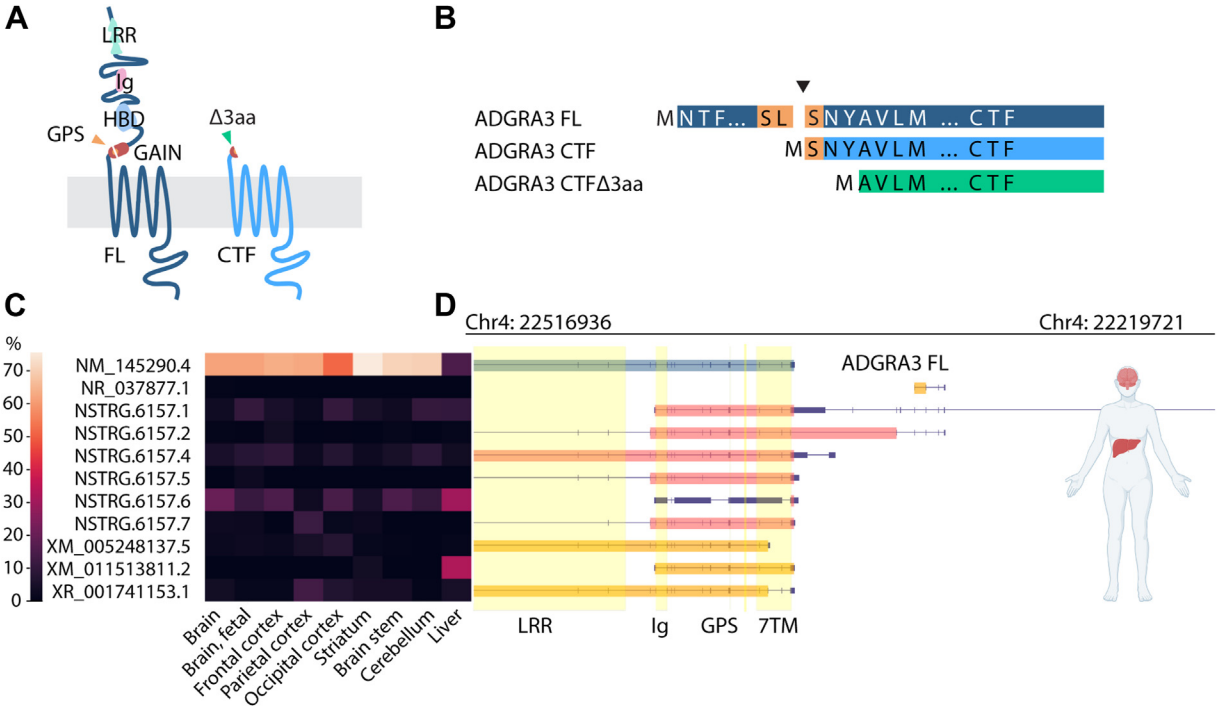

Figure 1. ADGRA3 transcript variant analysis and construct design. *A*, schematic outlining of the tertiary structure of the ADGRA3 full-length (FL) construct, based on the NM_145290.4 transcript variant and the corresponding C-terminal fragment (CTF) construct, truncated at the GPS. *Green triangle* symbolize the site of Δ3aa truncation of CTF. *B*, outline of the sequences of ADGRA3 constructs used throughout the study. The *triangle* depicts the site of CTF truncation between Ser^{736}-Leu^{737} and Ser^{738}. *C*, RNA-seq data from human brain and liver were analyzed for transcript variant disposition reference-guided transcript assembly with concepts of *de novo* by the pipeline described in Experimental procedures. The heat map shows the abundance of each transcript variant as a percentage of all variants according to the scale. NM_145290.4 is predominant. Novel accession numbers starting with "NSTRG" are not yet annotated in the NCBI database. *D*, visualization of the transcript variants at locus Chr 4: 22219721-22516936, showing the longest ORFs in *thick boxes* for novel (*red*) and database annotated (*orange*) transcripts. The predominant transcript variant NM_145290.4, containing 19 exons, is highlighted in *blue*. *Thinner purple boxes* depict 3′- and 5′ UTRs, and *dark blue lines* are introns. *Yellow columns* show regions encoding ADGRA3 protein domains and the GPCR proteolytic site (GPS). Aa, amino acid; Chr, chromosome; GAIN, GPCR autoproteolysis-inducing domain; HBD, hormone-binding domain; Ig, immunoglobulin-like domain; LRR, leucine-rich repeat domain; 7TM, seven helix transmembrane domain; TPM, transcripts per million.

tissue expression profiles (36–38), we sought the most prominent ADGRA3 transcript variant for further analysis. Therefore, we performed reference-guided transcript assembly in publicly available human RNA-seq datasets from eight regions of the brain and the liver of deeply sequenced (7–111 million reads per sample) RNA-seq data (39–41). The pipeline used for this assembly is delineated in the Experimental procedures section, with Gene Expression Omnibus accession numbers available in Table S1. We found eleven transcript variants that met the cutoff for being expressed significantly in at least one of the tissues (Fig. 1*C*). Of those, five variants are already annotated in the NCBI database (ORFs marked orange), and six were novel (ORFs marked red). One transcript variant (annotated NM_145290.4, ORF marked blue) presented with the highest expression over all analyzed brain regions, accounting for 51.6% to 75.5% (in brain occipital cortex and striatum, respectively) of the expressed variants, and showed high absolute expression levels (Table S2). This variant contains 19 exons and encompasses all the annotated domains of ADGRA3 (Fig. 1, *A* and *D*). In the liver, NM_145290.4 accounted for 15.1%, whereas the two major liver variants were NSTRG6157.6 and XM_011513811.2, accounting for 30.6% and 32.8% of total variant expression, respectively. However, upon examining the sequences, we found that NSTRG6157.6 is spurious, with only a very short ORF and no signal peptide. We predicted 1 hydrophobic stretch of signal peptide character in XM_011513811.2, yet short and of unknown targeting potential (Fig. 1*D*). Collectively, this highlighted NM_145290.4 as the most relevant and highest expressed ADGRA3 transcript variant in the analyzed human tissues.

Based on the dominance of the 19-exon transcript variant across the range of analyzed human tissues, we continued with NM_145290.4 as the template for our construct design for transient transfection of human cell lines, here referred to as ADGRA3 FL (Fig. 1, *A* and *B*). We truncated ADGRA3 FL at the predicted GPS cleavage site (marked in Fig. 1, *A* and *B* by orange color and a gap) to generate an ADGRA3 CTF construct for the signaling analysis (21). Further truncations were introduced to abolish the putative tethered agonist (ADGRA3 CTFΔ3aa) (Fig. 1, *A* and *B*, marked by green color).

Broad screen for G-protein activity downstream of ADGRA3

To assess the ability of ADGRA3 to activate heterotrimeric G proteins, we first screened for its capacity to engage each of the four major G protein–dependent pathways. G-protein engagement by ADGRA3 has been suggested from previous studies based on coimmunoprecipitation (20, 21), but the actual ability of ADGRA3 to activate G protein–dependent signaling has never been described. To address each of the G-protein families separately, we used a HEK293A-derived CRISPR knock-out cell line devoid of Gα subunits, $\alpha_{s/olf,\ z,\ q/11,\ 12/13}$ (HEK7GKO) (42) expressing solely Gα subunits of the $\alpha_{i/o}$ family. As a readout for pathway activity, we used four distinct luciferase reporter gene assays, which have been successfully used for profiling class A GPCRs and other aGPCRs to characterize constitutive (basal, ligand-independent) signaling downstream of heterotrimeric G-protein activation (43–45). In these reporter gene assays, luciferase is placed under the control of a specific transcription factor response element promoter, and receptor activity is quantified as a change in luminescence compared to empty vector control. We used the following four transcription factor systems: Nuclear factor of activated T cells (NFAT, controlled mainly by $G\alpha_{q/11}$), nuclear factor κ-light-chain-enhancer of activated B cells (NFκB, as readout mainly downstream of $G\alpha_{q/11}$ and $G\alpha_{12/13}$), serum response element (SRE, as readout mainly downstream of $G\alpha_{12/13}$ and $G\alpha_{q/11}$), and cyclic adenosine monophosphate (cAMP) response element (CRE, controlled mainly by $G\alpha_s$ and $G\alpha_i$. By reintroducing one Gα subunit at a time, using reporter gene assays in the HEK7GKO cells, we screened ADGRA3 FL and CTF constructs, for the G-protein selectivity. (Fig. 2*A*). As positive controls, we used receptors known to couple to the targeted Gα isoform in the HEK7GKO cells (Fig. S1) and as previously shown (42). We did not observe any significant activity changes upon transient expression of either of the two constructs in the NFAT or NFκB cotransfected with any Gα subunit and at relevant assay windows (44, 46) (Fig. 2, *B* and *C*). Compared to ADGRA3 FL, ADGRA3 CTF slightly decreased the SRE luminescence upon cotransfection with $G\alpha_{12}$ and $G\alpha_{13}$ (Fig. 2*D*). In the CRE reporter gene assay, both ADGRA3 FL and CTF decreased luminescence in $G\alpha_{olf}$-expressing cells (with the addition of Ric-8B to chaperone $G\alpha_{olf}$ expression) (Fig. 2*E*). As $G\alpha_{olf}$ is a member of the $G\alpha_s$ family of adenylyl cyclase-stimulating Gα subunits, the decrease in CRE activity suggests activation of endogenous $G\alpha_{i/o}$ proteins. By titrating in a $G\alpha_s$ subunit construct at two additional concentrations (100 ng and 200 ng, Fig. 2*F*), we confirmed that CRE activity was suppressed by both ADGRA3 FL and CTF, also when cotransfected with $G\alpha_s$ (Fig. 2*F*). Thus, the ADGRA3-mediated counteraction of $Ga_{olf/s}$ signaling to CRE-dependent transcription, suggests that ADGRA3 activates endogenous $G\alpha_i$ family proteins.

ADGRA3 signals through both G_i and G_s proteins

Next, we further investigated the $G\alpha_i$-mediated signaling elicited by ADGRA3 by cotransfecting the CRE-luciferase reporter gene with increasing plasmid amounts of either of the two ADGRA3 constructs (FL and CTF) into the HEK7GKO cell line. To elevate intracellular cAMP levels, the cells were preincubated with forskolin (50 μM), a direct activator of adenylyl cyclase, and transfected with C terminally truncated $G\alpha_s$ ($G\alpha_{s\Delta 10}$), which fully complements adenylyl cyclase activity to induce cAMP, but has abolished receptor coupling (44). The dopamine receptor D_2 served as a positive control for $G\alpha_i$ coupling. We found that ADGRA3 FL and CTF decreased the forskolin-induced CRE signal in a gene dose-dependent manner, supporting the concept of constitutive receptor activity toward $G\alpha_{i/o}$ proteins (Fig. 3*A*). The two receptor constructs were expressed at the cell surface at comparative levels (Fig. S2, *A* and *B*). To rule out a cellular bias of the CRISPR cell line (HEK7GKO) in driving the $G\alpha_{i/o}$ protein activity, we repeated the experiment in WT HEK293T cells. Again, ADGRA3 FL and, to a greater extent, CTF decreased CRE

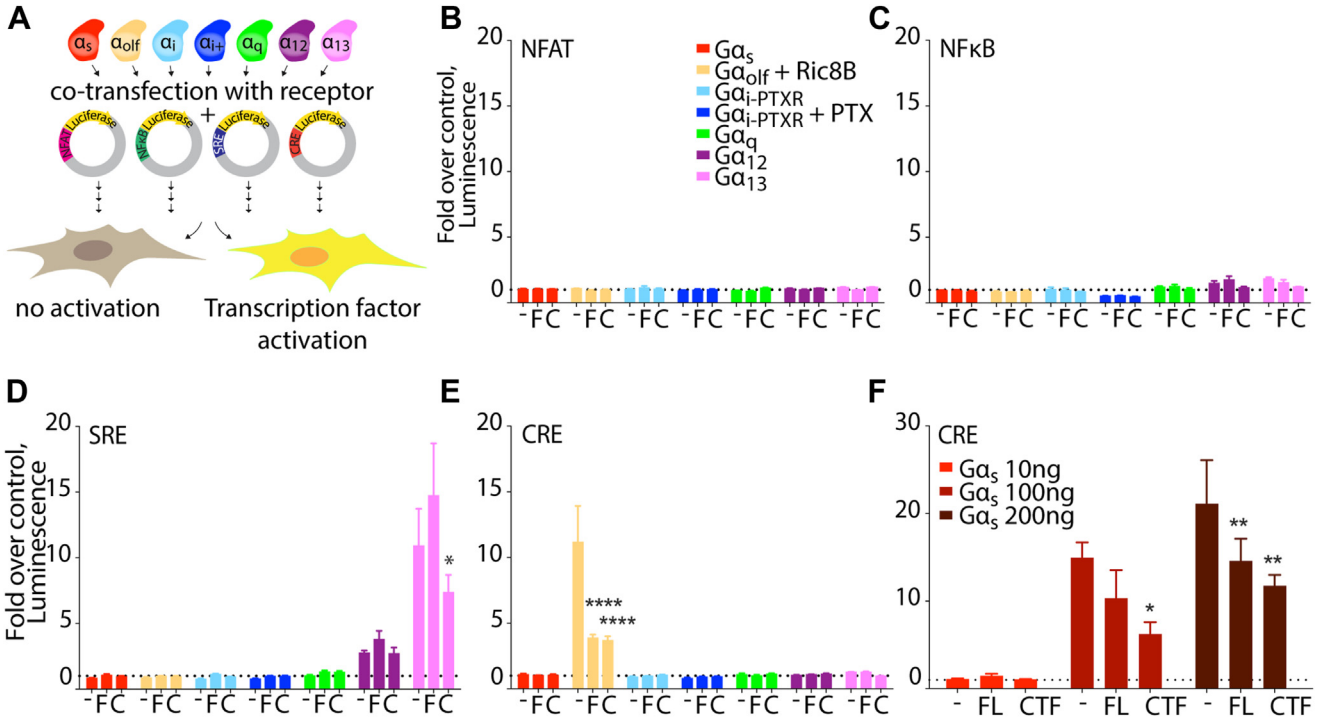

Figure 2. Decreased CRE response in ADGRA3-expressing cells in a downstream readout of Gα protein screening. *A*, schematic of the Gα protein screening in HEK7GKO cells (Gα subunit-depleted, except for $G\alpha_{i/o}$). One reporter gene plasmid (300 ng) containing luciferase under the control of a transcription factor response element (NFAT/NFκB/SRE/CRE) was cotransfected with ADGRA3 FL, CTF or empty vector, as well as one Gα subunit at a time ($G\alpha_{s/olf+Ric8B/i\text{-}PTXR/i\text{-}PTXR+PTX/q/12/13}$) (10 ng). Downstream pathway activity was measured as an increase (or decrease in the case of $G\alpha_i$ family proteins) in luminescent emission signal at 525 nm. *B–E*, screening results stratified by each transcription factor reporter gene. *F*, CRE reporter gene assay with increased amounts of $G\alpha_s$ cDNA (10 ng, 100 ng, 200 ng) in HEK7GKO cells, cotransfected with ADGRA3FL, CTF, or empty vector. *B–F*, data presented as fold over no G protein control (*dashed line*) from three (*B–E*) or five (*F*) independent experiments in technical triplicates ± SEM. Statistics: *B–F*, two-way ANOVA, followed by Tukey's correction for multiple testing. *Asterisks* denote comparisons to no G protein empty vector control: $^*p < 0.05$, $^{**}p < 0.01$, and $^{****}p < 0.0001$. The full result of the statistical analysis can be found in Table S3. CTF, C-terminal fragment; CRE, cAMP response element; FL, full length; NFAT, nuclear factor of activated T cells; NFκB, nuclear factor kappa-light-chain-enhancer of activated B cells; PTX, pertussis toxin; PTXR, pertussis toxin resistant; Ric8B, RIC8 guanine nucleotide exchange factor B; SRE, serum response element.

activity even when the full panel of endogenous Gα subunits was present (Fig. 3*B*). Consulting the area under the curve (AUC), the two graphs (bar plots Fig. 3, *A* and *B*) show very similar patterns between the two cell types.

We proceeded to omit the forskolin-induced prestimulation of adenylyl cyclase. In this setting, using HEK293T cells with endogenously expressed $G\alpha_s$ and $G\alpha_i$, ADGRA3 CTF significantly increased the CRE luminescence compared to empty vector transfections (Fig. 3*C*). Again, the CTF construct appeared more active than FL ADGRA3, only trending to increase the CRE luminescence. The constitutively activated Epstein-Barr virus-encoded receptor, BILF1, was included as a positive control for Gi activity (47, 48), and negatively impacted the CRE response in comparison to empty vector control ($p = 0.053$) (Fig. 3*C*). Collectively, this suggests Gs and Gi activity of ADGRA3 in this setting without a prestimulatory pressure on adenylate cyclase.

To explore the balance between the apparent divergent Gs-Gi activities, we decreased the forskolin concentration from 50 μM to 5 μM, a concentration eliciting a submaximal CRE response, in the HEK293T cell line (Fig. S2*C*). Under these conditions, with reduced adenylyl cyclase activity, ADGRA3 FL decreased the CRE luminescence comparable to that seen after the high forskolin preincubation (Fig. 3*D*), and so did the positive control, BILF. In contrast, the CRE response downstream from the CTF oscillated around zero at low forskolin level (Fig. 3*D* gene dose and area under the curve), suggesting a stronger Gs relative to Gi balance of CTF (*i.e.*, in the absence of NTF) than FL receptor.

Knocking out $G\alpha_s$ abolishes the positive CRE signal and increases CRE inhibition

To confirm $G\alpha_s$-mediated increase in CRE activity from ADGRA3, we used a HEK293A-derived CRISPR KO cell line devoid of the $G\alpha_s$ family subunits (HEKΔGs) (49) and repeated the CRE reporter assay. As a positive control for $G\alpha_s$-mediated CRE signaling, we included GPR119, a cannabinoid receptor-like class A GPCR (50, 51). In the parental cell line, expressing the full panel of Gα subunits, we saw a strong positive CRE response, even at low gene doses, from GPR119, which was completely abolished in the HEKΔGs cells (Fig. 4*A*). For ADGRA3 FL, we observed an oscillation around baseline in the parental cell line supplemented with low (5 μM) forskolin, which was downshifted in the HEKΔGs cells, reflective of increased $G\alpha_i$ activity upon

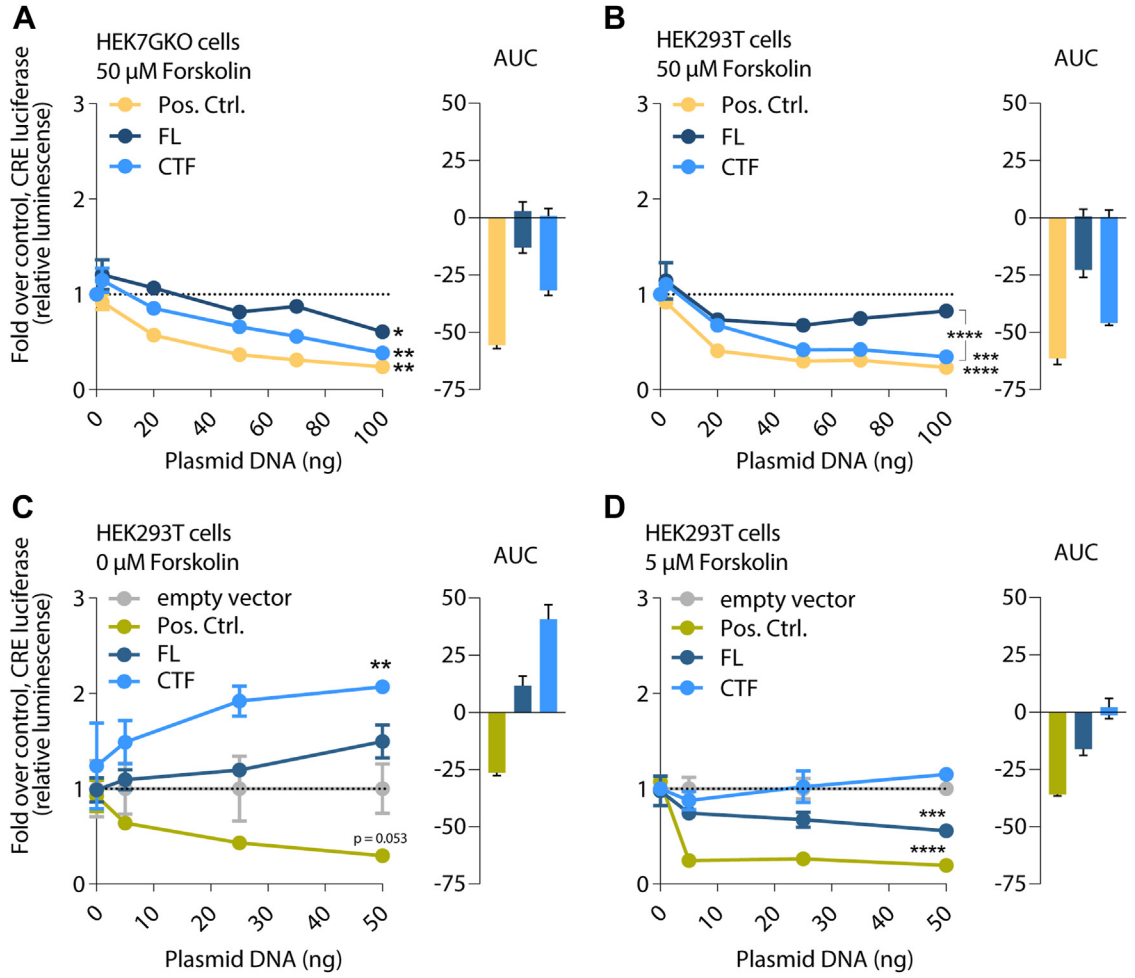

Figure 3. ADGRA3 signals *via* Gα_i and Gα_s with a stronger activity of CTF relative to FL receptor. *A–D*, CRE reporter gene assays with increasing gene doses of ADGRA3 FL, CTF, and positive control for Gα_i activity; (*A*) HEK7GKO cell line or (*B*) HEK293T cells were cotransfected with G$\alpha_{s\Delta 10}$ (*C* terminally truncated Gα_s, which is cAMP-inducing, but unable to couple to G proteins) and pretreated with 50 µM forskolin (*high*) to stimulate adenylyl cyclase. D_2R serves as a control for constitutive Gα_i activity. *C*, HEK293T cells received no adenylyl cyclase stimulation. *D*, HEK293T cells prestimulated with 5 µM forskolin (*low*). *C* and *D*, BILF1 serves as a control for constitutive Gα_i activity. *A–D*, luminescence was measured at 525 nm. Data are presented as mean fold over empty vector control ± SEM of three independent experiments of technical triplicates. *A* and *B*, *dotted line* displays 0 ng ADGRA3 cDNA point (100 ng empty vector); cDNA weight was adjusted to 100 ng/well with empty vector during transfection. *C* and *D*, empty vector was tested experimentally in parallel to ADGRA3 with increasing gene dose (0–50 ng). cDNA weight was not adjusted for each gene dose, but data were normalized to the corresponding empty vector cDNA weight. *A–D*, area under the curve (AUC) is visualized next to each graph ± standard error. Statistics: (on the last data point) one-way ANOVA followed by Tukey's correction for multiple testing. *Asterisks* show comparison to empty vector control unless otherwise indicated by brackets; $*p < 0.05$, $**p < 0.01$, $***p < 0.001$, and $****p < 0.0001$. The full result of the statistical analysis can be found in Table S3. AUC, area under the curve; CRE, cAMP response element; CTF, C-terminal fragment; D_2R, dopamine receptor D_2; FL, full length; PTX-S1, pertussis toxin subunit 1.

Gα_s depletion, albeit signaling was weak (Fig. 4*B*). For CTF, we observed an increase in the CRE signal at the same low forskolin level (Fig. 4*C*) in the parental cell line (with Gα_s), however, in the Gα_s-depleted cells, this increase was abolished, and the CRE luminescence further decreased, again reflecting more Gα_i signaling activity in the absence of Gα_s. This suggests that ADGRA3 CTF balances toward Gs signaling in HEK293A WT cells with this level of basal CRE activity.

Cellular differences in CRE response reveal ADGRA3 Gs activity requires a certain pre-pressure on Gs

Noticeably, we observed differences in the CRE responses, both in basal levels and, in particular, in response to forskolin between the different cell lines (Fig. S3). The HEK293A cells had a mean basal CRE response of ∼1000 relative luminescence units, which increased around 30-fold upon the addition of 5 µM forskolin. The basal CRE response was reduced to half in HEKΔGs cells (derived from HEK293A) and increased less than 3-fold with the same forskolin addition. We attribute the modest CRE response in the HEKΔGs to the hampered Gα_s signaling axis. However, comparing the two cell lines with WT levels of G proteins, we found that HEK293T had a much higher basal CRE activity, almost six times higher than HEK293A. Adding 5 µM forskolin increased this further by 20-fold. Our results suggest that ADGRA3 is more prone to mediate an increase in CRE response in cells with a certain prepressure on the Gs signaling axis, that is, HEK293A supplemented with 5 µM forskolin, or unstimulated HEK293T cells. If the initial CRE activity is higher than the "Gs signaling

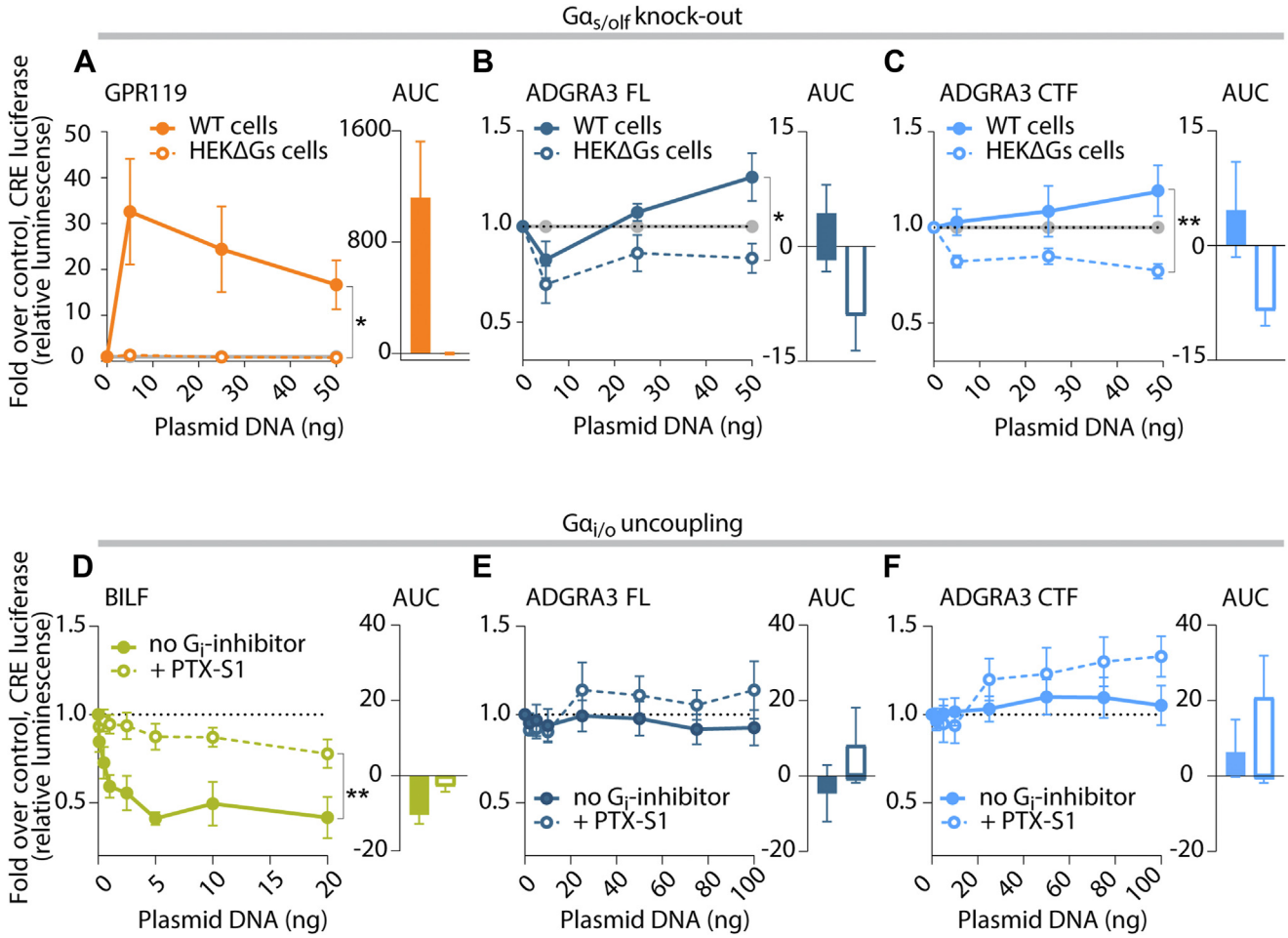

Figure 4. Modulation of cellular $G\alpha_{s/olf}$ or $G\alpha_{i/o}$ confirms ADGRA3 signaling through both axes. *A–C*, CRE reporter assays in HEK293A "parental" cells and CRISPR-engineered $G\alpha_{s/olf}$ knock-down cell line, HEKΔGs. *A*, GPR119 serves at positive control for $G\alpha_s$-coupled signaling. *B*, ADGRA3 FL and (*C*) CTF gene doses in the presence of 5 μM forskolin (*low*). *D–F*, CRE reporter assays in HEK293T cells with or without $G\alpha_i$ uncoupling by PTX-S1 cotransfection and in the presence of 5 μM forskolin (*low*). *D*, BILF serves as control for constitutive $G\alpha_i$ activity. Gene doses of (*E*) ADGRA3 FL and (*F*) CTF. *A–F*, Data are presented as mean fold over empty vector control ± SEM. *A–C*, empty vector was tested experimentally in parallel to ADGRA3 with increasing gene dose (0–50 ng), and data were normalized to the corresponding empty vector data point, n = 4. *D–F*, *dotted line* displays 0 ng ADGRA3 cDNA point (100 ng empty vector) and total cDNA weight was adjusted to 100 ng/well with empty vector during transfection, n = 7. *A–F*, area under the curve (AUC) is visualized next to each graph ± standard error. Statistics: (on last data point) (*A–C*) one-way ANOVA with Tukey's *post hoc* test and (*D–F*) Student's paired two-tailed *t* test on plotted data. *$p < 0.05$ and **$p < 0.01$. The full result of statistical analysis can be found in Table S3. AUC, area under the curve; PTX-S1, pertussis toxin subunit 1; FL, full length; CTF, C-terminal fragment; CRE, cAMP response element.

zone", as in HEK293T cells stimulated with 5 or 50 μM forskolin, ADGRA3 switches to $G\alpha_i$ signaling, decreasing the CRE luminescence (Fig. S3).

Inhibition of $G\alpha_i$ ablates the CRE signal decrease

To control for $G\alpha_i$ coupling, we exploited *Bordetella pertussis* toxin (PTX) that ADP-ribosylates all members of the $G\alpha_{i/o}$ family (except for $G\alpha_z$, which lacks a cysteine residue four positions from its C terminus), thereby uncoupling them from their receptors (52). In the presence of forskolin, the decrease in CRE signaling elicited by the $G\alpha_i$-coupling receptor, BILF1, was ablated, as shown by a "flattening" of the curve, when the active S1 subunit of PTX (PTX-S1) was coexpressed (Fig. 4*D*). Having verified that the assay worked as expected, we repeated the setup with increasing ADGRA3 FL gene dose, and again we observed a CRE response oscillation just below baseline in the cells with low forskolin, but upon PTX-S1 cotransfection the CRE signal was up-shifted (Fig. 4*E*). Similarly, increasing gene dose of ADGRA3 CTF, in the presence of low forskolin, showed a CRE activity just above baseline which increased upon $G\alpha_i$-uncoupling by PTX-S1, supporting Gs activity in the absence of an active $G\alpha_i$ (Fig. 4*F*). Collectively, our data suggest that ADGRA3 is capable of signaling through both the Gi and Gs axes to modulate CRE activity and that CTF shows a stronger signaling response than FL.

Truncating the tethered agonist of ADGRA3 abolishes G protein–mediated signaling

For several aGPCRs, the sequence immediately downstream from the GPS cleavage site works as an intramolecular tethered agonist to activate downstream signaling (28–31). Since we detected a difference in the G-protein signaling response of the artificially designed CTF compared to ADGRA3 FL, we addressed the role of the tethered agonist on ADGRA3 signaling properties. We deleted the first three amino acid

residues after the GPS motif in the CTF construct (CTFΔ3aa) (Fig. 1, *A* and *B*) (29) and tested the activity using the CRE reporter gene assay. In contrast to the CTF construct with an intact tethered agonist, CTFΔ3aa did not increase the CRE luminescence with increasing receptor gene dose (Fig. 5*A*). After low forskolin preincubation (5 μM), the elevated CRE response by CTF, and following shift upward by PTX-S1 cotransfection, was not copied by the truncated CTFΔ3aa (Fig. 5*B* with data reprinted from Fig. 4*F* for comparison), suggesting that the three-amino-acid deletion abolished CRE response. This indicates that for ADGRA3 CTF, the sequence corresponding to the class-defined tethered agonist is pivotal for its G protein–mediated signaling.

Gi-protein coupling by ADGRA3 does not depend on cellular DVL expression

Having established that ADGRA3 engages both Gs and Gi signaling pathways and considering that previous studies show DVL redistribution by the receptor (11, 21), we next investigated whether the two pathways might be interrelated. To answer this question, we addressed the Gi activation by ADGRA3 in HEK293T cells depleted for all DVL isoforms (ΔDVL1-3 cells) (34) by applying a G protein activity sensor bioluminescence resonance energy transfer (BRET) system based on a tricistronic vector (G-CASE), which has been described for other constitutive active GPCRs (53, 54). Upon receptor coupling, the heterotrimeric G protein complexes dissociate, and the BRET signal between nLuc-tagged Gα and cp-Venus–tagged Gγ decreases (Fig. 6*A*). We addressed the three main $G\alpha_i$ proteins ($G\alpha_{i1-3}$) and found that ADGRA3 CTF was able to engage all $G\alpha_i$ proteins ($G\alpha_{i1}$, $G\alpha_{i2}$, and $G\alpha_{i3}$) as seen by a significant decrease in the BRET ratio compared to empty vector control (Fig. 6, *B-D*). The FL receptor, ADGRA3 FL, only elicited BRET sensor activity when coexpressed with $G\alpha_{i3}$. As a positive control, we used the histamine receptor type 3 (H_3R), based on its constitutive $G\alpha_i$ coupling (53). Collectively, this suggests that ADGRA3 is capable of activating Gai signaling axes independently of DVL presence.

ADGRA3 does not engage WNT/β-catenin signaling

DVL is an important early mediator of both β-catenin–dependent and β-catenin–independent WNT signaling pathways (28), and ADGRA3 was previously suggested to inhibit WNT/β-catenin signaling at the β-catenin transcriptional level in WNT3A-stimulated cells (11, 15, 21). To address the function of ADGRA3 in cells without a prevailing pressure on the WNT signaling pathways, we investigated the transcriptional activation downstream of β-catenin and TCF/LEF (T-cell factor/lymphoid enhancer factor) using a TOPFlash reporter gene assay in the absence of frizzled expression (ΔFZD_{1-10} cells) (55). Compared to the empty vector control, we were not able to detect an increase in the TOPFlash signal when cotransfecting with ADGRA3 FL or CTF (Fig. 7). As expected, FZD_4 induced an increase in the β-catenin-regulated and TCF/LEF-dependent transcriptional activation, which was potentiated by the addition of its ligand WNT3A (Fig. 7).

Discussion

Here, we worked with the most abundant transcript variant of ADGRA3 and systematically screened for pathway activation through distinct heterotrimeric G proteins. Our expression system included receptor gene overexpression and WT and engineered KO cell lines to study the influence of other previously reported pathways on G-protein signaling of ADGRA3.

The signal transduction from the 33 members of the aGPCR class spans both G protein–coupled and alternative pathways. Receptor-induced G-protein activation has been reported for

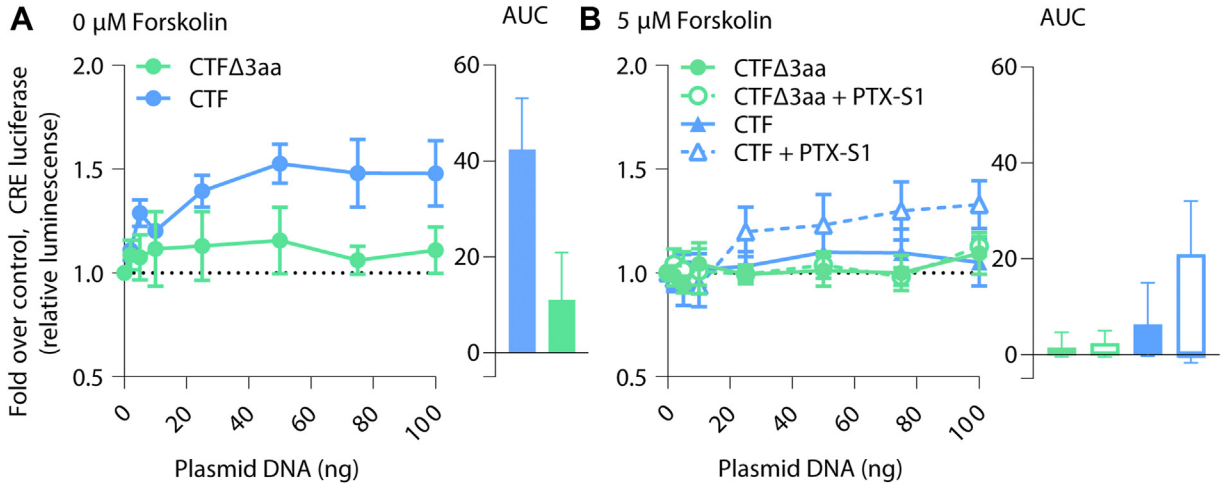

Figure 5. Truncation in the ADGRA3 tethered agonist sequence abolishes G-protein activation. *A*, CRE reporter gene assay with increasing gene-doses of ADGRA3 CTF and CTFΔ3aa in HEK293T cells in the absence of forskolin. *B*, CRE luminescence from ADGRA3 CTFΔ3aa after prestimulation with 5 μM forskolin (*low*), with and without $G\alpha_{i/o}$ uncoupling by PTX-S1 cotransfection. ADGRA3 CTF CRE response reprinted from Fig. 4*F* (*sky blue triangles*) for comparison. Data are presented as mean fold over empty vector control (*dotted line*) ± SEM, n ≥ 4. Area under the curve (AUC) is visualized next to each graph ± standard error. Statistics: Student's paired two-tailed *t* test on plotted data (on last data point). The full result of statistical analysis can be found in Table S3. AUC, area under the curve; CRE, cAMP response element; CTF, C-terminal fragment; FL, full length; PTX-S1, pertussis toxin subunit 1.

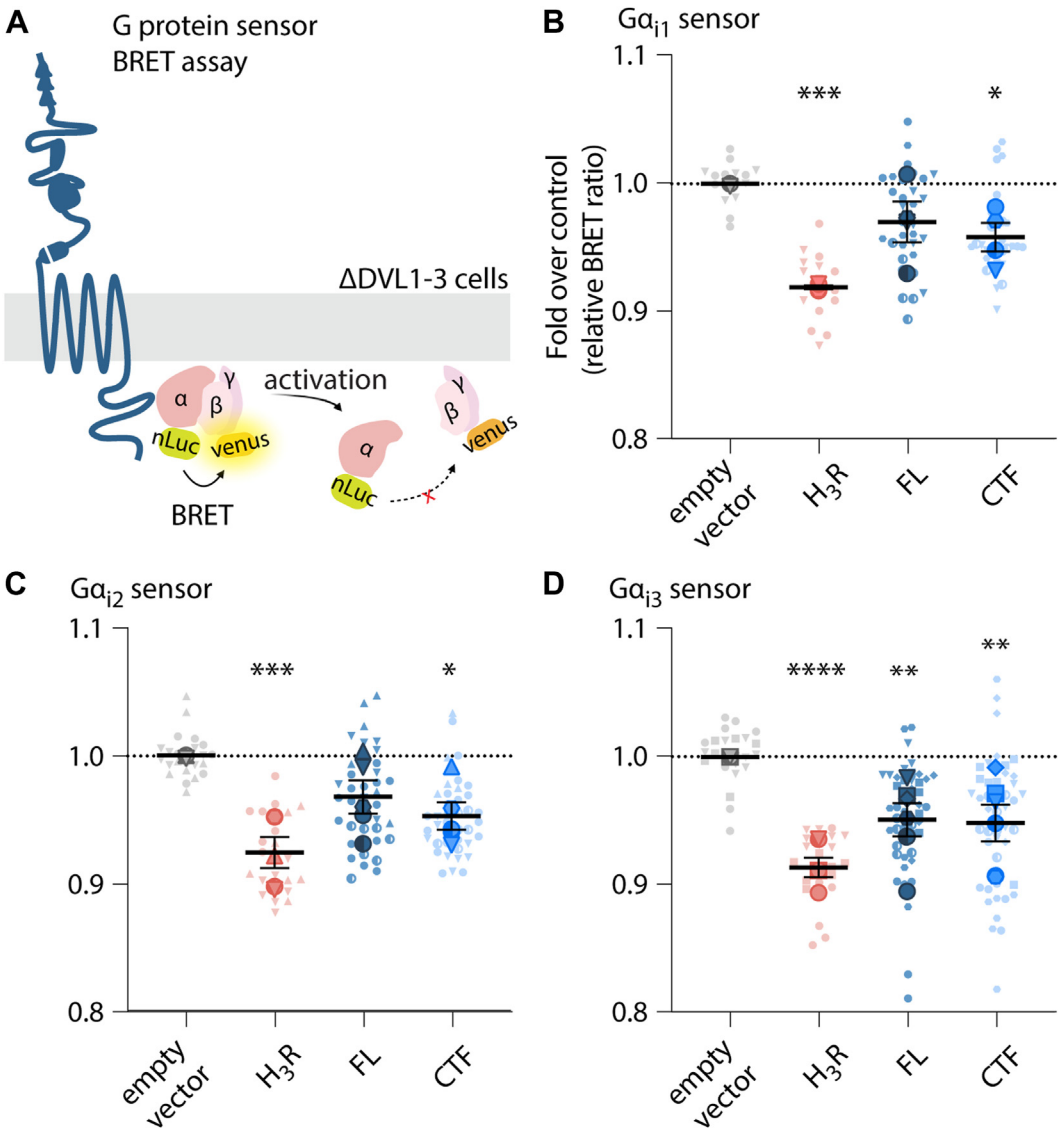

Figure 6. G-protein activation by ADGRA3 CTF is sustained in the absence of DVL1-3. *A*, schematic outline of G-protein activity BRET sensor system. Upon activation, the heterotrimeric G-protein complex dissociates, and the BRET signal between nLuc-tagged Gα (donor) and cp-Venus–tagged Gγ (acceptor) ceases. The BRET sensors are cotransfected with the depicted receptors into ΔDVL1-3 cells. *B–D*, $G\alpha_{i1-3}$ sensors cotransfected with ADGRA3 FL and CTF. H_3R serves as positive control for constitutive $G\alpha_i$ activity. Empty vector control is pcDNA3.1+. Data are presented as BRET ratio, emission [venus/nLuc], shown as fold over empty vector control for each transfection in "SuperPlots" (85): *Small, light-colored data points* show the distribution of technical replicates, and *large, darker data points* on *top* show the biological replicates (n ≥ 4) and are the basis of mean ± SEM overlayed and statistical testing. Different data point shapes visualize which technical and biological replicates belong to the same experiment. Statistics: one-way paired ANOVA followed by Tukey's correction for multiple testing. *Asterisks* show the comparison to empty vector control; *$p < 0.05$, **$p < 0.01$, ***$p < 0.001$, and ****$p < 0.0001$. The full result of the statistical analysis can be found in Table S3. BRET, bioluminescence resonance energy transfer; CTF, C-terminal fragment; DVL, disheveled; FL, full length; H3R, histamine receptor type 3.

more than half of the aGPCRs, and typically, one receptor pleiotropically engages more than one G protein (2, 28). For example, simultaneous $G\alpha_s$ and $G\alpha_i$ activation has been shown for ADGRL1 (latrophilin1) and ADGRV1 (GPR98), which also signal through $G\alpha_q$, and for ADGRG6 (GPR126) (56–60). We find that ADGRA3 engages both Gs and Gi. The enhanced Gs activity in the presence of PTX, combined with the enhanced $G\alpha_i$ in the absence of $G\alpha_s$, supports this dual coupling and the delicate balance between Gs and Gi for ADGRA3. The phenomenon that inhibition of the inhibitory subunit ($G\alpha_i$) by PTX strengthens the outcome of the signaling from Gs is not a novel phenomenon. It was previously described in, for instance, the β_2-adrenergic receptor that coupled effectively to the same two Ga subunits and hence both activate and inhibit the adenylate cyclase *via* coupling to $G\alpha_s$ and $G\alpha_i$, respectively (61, 62), like observed here for ADGRA3 (Figs. 3 and 4).

Although the CRE response downstream of ADGRA3 is weak, we find that the CTF elicits a slightly higher signal than ADGRA3 FL (*e.g.*, Fig. 3*B*), in concordance with observations from other aGPCRs (27). The ability of ADGRA3 CTF to decrease the SRE response slightly in the presence of $G\alpha_{13}$ suggests some level of pathway crosstalk at the gene expression level. Furthermore, we find the signaling to be cell-subtype–dependent (HEK293T *versus* HEK7GKO with HEK293A as

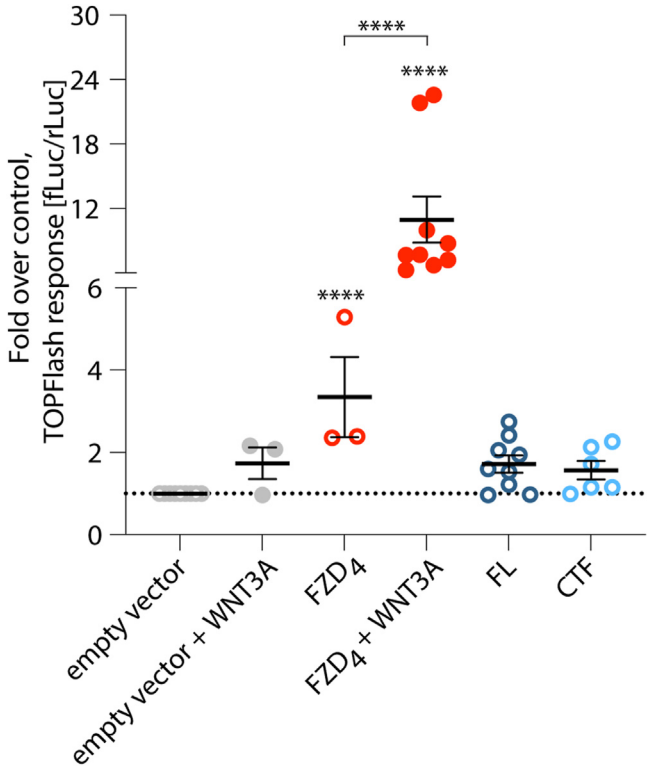

Figure 7. ADGRA3 does not engage WNT/β-catenin signaling. Quantification of the β-catenin responsive TOPFlash assay in ΔFZD_{1-10} cells, co-transfected with ADGRA3 FL, CTF or FZD_4. FZD_4 serves as positive control and is shown with or without 1 μg/ml WNT3A ligand stimulation. TOPFlash signal was read as [580 nm (fLuc)/480 nm (rLuc)]. One datapoint is the average of one independent transfection, n = 3–9 transfections, and data are presented as fold over empty vector control (pcDNA) with mean ± SEM indicated. Statistics: one-way ANOVA followed by Tukey's correction for multiple testing. Asterisks denote comparisons to negative control, unless brackets indicate otherwise; $^{****}p < 0.0001$. The full result of the statistical analysis can be found in Table S3. CTF, C-terminal fragment; FL, full length; fLuc, firefly luciferase; FZD, frizzled; rLuc, renilla luciferase.

parental cell line), thus reflected by the G-protein composition and possibly pathway modulators, endogenously and exogenously expressed in the cell lines.

We find the G-protein activation by ADGRA3 CTF to depend on the three amino acid positions after the homologous position of the aGPCR-conserved GPS cleavage site (Fig. 5, *A* and *B*). This is consistent with recent cryogenic electron microscopy structures of several aGPCRs coupled to their respective G proteins, showing the tethered agonists embedded within a typical seven transmembrane domain orthosteric site (63–66). With the increased G-protein activation downstream from the CTF relative to ADGRA3 FL, one could speculate that CTF also elicits a tethered agonist–enhanced coupling. It should, however, be emphasized that it remains to be proven that ADGRA3 is cleaved at the non-canonic GPS (SL|S/G), although one study suggests so (21).

The implemented transcription factor- and BRET-based experiments allow us to detect downstream signal amplification and loss of donor-energy transfer, respectively, but do not reveal the subcellular location of the receptor–effector interactions. Previous work shows that ADGRA3 internalizes constitutively in a β-arrestin–independent but clathrin-mediated manner (67). It was also shown by microscopy that ADGRA3 recruits DVL to distinct plasma membrane subdomains in zebrafish embryos and that Dlg1 localized ADGRA3 to the basolateral membrane of canine kidney epithelial cells (11, 21). Further studies are therefore needed to decipher the potential compartmentalized signaling of ADGRA3.

ADGRA3 belongs to family III of aGPCRs, comprising ADGRA1 (GPR123) and ADGRA2 (GPR124). Whereas ADGRA2 has never been shown to couple to heterotrimeric G proteins, it has been extensively studied for its role in the assembly of a complex signalosome of WNT7A/B-FZD-DVL/Dlg-LRP5/6 (low-density lipoprotein receptor-related protein 5/6)-in the blood-brain barrier (6, 9, 55, 68–72). ADGRA1 is unique in having a very short N terminus and no GPCR autoproteolysis-inducing domain. It has received limited attention regarding signaling properties but was found to coexpress and localize with $G\alpha_{i1-3}$ in a study of human pluripotent stem cell reprogramming (7). Thus, it resembles ADGRA3 according to previous data and our findings (*e.g.*, Fig. 3*B*) (21).

Early studies show that ADGRA3 modulates the WNT PCP pathway in zebrafish (11). Furthermore, ADGRA3 colocalizes with Dlg1 in cell polarity regulation (21) and was found to interact with the receptor-like tyrosine kinase in an affinity proteomics study (73). Receptor-like tyrosine kinase is a WNT coreceptor and mediator of polarized cell migration during development (74, 75). It is tempting to imagine an ADGRA3 signalosome with DVL and/or Dlg as scaffolding proteins based on previous interactions (21, 23), evolving around noncanonical WNT/PCP signaling pathway components, but this remains to be elucidated. Furthermore, the observation that ADGRA3 does not depend on DVL for Gi-protein signaling (Fig. 6, *B–D*) suggests that the two signaling pathways entailing G-protein activation and DVL recruitment are unrelated, implying the existence of a complex signalosome of dual function or that the two processes are independent (76).

Few other aGPCRs are implicated in WNT signaling cascades. For instance, ADGRE5 (CD97) interacts with β-catenin in adherence junctions of normal and transformed colorectal cells, yet the receptor does not regulate β-catenin-TCF/LEF–mediated transcriptional activity (77). ADGRG1 (GPR56), on the other hand, activates TCF transcription (78). Assay for transposase-accessible chromatin in acute myeloid leukemia samples revealed that high ADGRG1 level correlated with both WNT and Hedgehog signal partway activity and that ADGRG1 suppression led to downregulation, at the RNA level, of "WNT-related" genes, including *DVL1* (79). We could not detect any constitutive activation of TCF transcription (TOPFlash reporter) by ADGRA3 (Fig. 7).

In a biological context, ADGRA3 was initially identified as a marker of undifferentiated spermatogonial progenitors (17). Since then, it has been shown that ADGRA3 is expressed in both mammary progenitors (13), lacrimal gland progenitors (19), in male and female reproductive tract development (12,

18), in osteoclastogenesis (24), in the brain with upregulation after brain injury (10), as well as playing a role in several cancers (13–16). Collectively, this suggests that ADGRA3 is an important player in orchestrating cell and tissue homeostasis in both development and regeneration. Here, we add functional and dual G protein–mediated signaling of ADGRA3 as a potential contributor to its biological effects.

Experimental procedures

Materials

Dulbecco's modified eagle medium (DMEM) + high glucose (GlutaMAX), OptiMEM + GlutaMAX, Hank's balanced salt solution + $CaCl_2$ + $MgCl_2$ ($HBSS^{++}$), and readily heat-inactivated fetal bovine serum (FBS) were from Gibco. Penicillin-streptomycin and PBS + $CaCl_2$ + $MgCl_2$ (PBS^{++}) were from the in-house vendor ("Sterilcentralen"). Dulbecco's PBS was from Corning. FBS (non-heat-inactivated) was from Sigma Life Science. Poly-D lysine hydrobromide (PDL) and 37% formaldehyde were from Sigma-Aldrich. Enzyme-free cell dissociation solution was from MilliporeSigma. Trypsin-EDTA was from VWR. Lipofectamine2000 was from Invitrogen. SteadyLite reporter gene assay system (Firefly d-luciferin) was from PerkinElmer. HaloTag NanoBRET 618 ligand was from Promega. Coelenterazine-h and firefly d-luciferin were from NanoLight Technology. Enzyme-free cell dissociation solution and bovine serum albumin (BSA) were from MilliporeSigma. Recombinant human WNT3A were from R&D Systems/Bio-techne (#5036-WN). WNT3A and vehicle control were dissolved in filter-sterilized 0.1% BSA in PBS (WNT3A) or HBSS (vehicle) and kept on ice when handled.

Plasmids

ADGRA3 FL, ADGRA3 CTF, and ADGRA3 CTFΔ3aa (all harboring an N-terminal Flag-tag; DYKDDDDK) were synthesized by GenScript and were based on the sequence of NM_145290.4 cloned into a pcDNA3.1+ vector background (used in Figs. 5 (CTFΔ3aa), 6, 7).

Codon-optimized constructs of ADGRA3 FL and CTF were used in Figures 2–5 (CTF) and 6 and were obtained from GenScript, carrying an N-terminal Flag-tag (DYKDDDDK) and a C-terminal 1D4-tag, as well as an artificial signal peptide (aSP; originating from influenza hemagglutinin) instead of the inherent one.

aSP: ATG AAG ACT ATT ATC GCA CTG AGC TAC ATT TTC TGC CTG GTG TTC GCT. The C-terminal 1D4-tag on these constructs was removed by Quikchange-PCR using the following primers:

Forward: GTG GAA ACA CGA GAC CAC AGT GTG AGG GCC CGT TTA AAC CCG C.

Reverse: GCG GGT TTA AAC GGG CCC TCA CAC TGT GGT CTC GTG TTT CCA C.

The G_{i1}, G_{i2}, and G_{i3} protein sensors (called G-CASE (53)) BILF construct (47) and $Ga_{s\Delta 10}$ construct (44) were generated and authenticated as described elsewhere.

All sequences were confirmed with Eurofins Genomic's DNA sequencing service.

Data processing and transcript assembly

We obtained several deep sequenced RNA-seq datasets (GSE101521, GSE138734, GSE174478) from the Gene Expression Omnibus public dataset (Table S1). Only paired-end RNA-seq samples were included, and datasets generated without random primers were excluded. The resulting datasets included 132 brain tissue samples and 102 liver tissue samples. The raw data was mapped against the hg38 human genome using STAR (version 2.7.6a; https://bioweb.pasteur.fr/packages/pack@STAR@2.7.6a) (80) with default parameters. After sorting with SAMtools (version 1.9; https://www.htslib.org/) (81), the mapped reads were assembled into transcripts and quantified by StringTie (version v2.1.3b; https://ccb.jhu.edu/software/stringtie/) (82). StringTie parameters "read coverage" (-c), "transcript length" (-m), and "bases on both sides of a junction a spliced read has to cover" (-a) were set to minimal values to avoid missing transcripts and generating a bias. The parameter "fraction of the most abundant transcript at one locus" (-f) was lowered from the default (0.01) to 0. For all other StringTie parameters, default values were used. StringTie merge mode, which provided the reference annotation (-G), was used to generate a global, unified set of transcripts across RNA-seq samples. Quantification of the abundance of the input transcripts was then performed using parameters "expression estimation mode" (-e) and the beforehand generated merged "reference annotation transcripts" (-G). For the visualization, the longest ORF was identified for each transcript and translated to protein sequence with the Python package Biopython (version 1.80; https://biopython.org/) (83). The transcript with the longest protein sequence was then screened for protein domains with InterProScan (version 5.60–92.0; https://www.ebi.ac.uk/about/news/tag/interpro/) (84) against the Pfam database (-appl).

Cell culture and transient transfection

HEK293T cells were obtained from ATCC (#CLR-3216). Additional cells lines with targeted gene-deletion *via* CRISPR-Cas9; HEK293A with targeted deletion of *GNAS*, *GNAL*, *GNAQ*, *GNA11*, *GNA12*, *GNA13*, and *GNAZ* (G protein knockouts, HEK7GKO); HEK293A with targeted deletion of *GNAS*, *GNAL* (HEKΔGS); HEK293T with targeted deletion of *FZ1*, *FZ2*, *FZ3*, *FZ4*, *FZ5*, *FZ6*, *FZ7*, *FZ8*, *FZ9*, *FZ10* (FZD knockouts, $\Delta FZD_{1\text{-}10}$); and HEK293T with targeted deletion of *DVL1*, *DVL2*, and *DVL3* (DVL knockouts, ΔDVL1-3), were derived, authenticated, and propagated as described elsewhere (34, 42, 49, 55).

All cell lines were propagated in cell culture flasks in a growth medium containing DMEM high glucose medium supplemented with 10% (FBS) and 1% penicillin-streptomycin and were maintained at 37 °C in a 5% CO_2 humidified incubator. FBS was heat-inactivated at 56 °C for 30 min if not readily heat-inactivated by the manufacturer. During seeding or passage, the cells were detached using trypsin-EDTA. The

absence of *mycoplasma* contamination was routinely checked using the MycoAlert *Mycoplasma* Detection Kit (BioNordika). The cells were transiently transfected using Lipofectamine2000 in Opti-MEM reduced serum medium according to the manufacturer's recommendations. For transfection of cells in suspension, the cells were seeded onto white bottom/white wall microtiter plates, precoated with 20 μg/ml PDL for 20 min, and washed twice with PBS before cell seeding unless otherwise stated.

Gα subunit screen and transcription factor reporter gene assays

Gα subunit screen

HEK7GKO cells were plated in 12-well culture plates at a density of 3 to 4 × 10^5 cells/well and incubated overnight. Twenty four hours after seeding, cells were transiently transfected using Lipofectamine2000 (2.3 μl/1 μg plasmid DNA) and a total of 800 ng plasmid DNA as follows: 300 ng of reporter (CRE-Luc/SRE-Luc/NFκB-Luc/NFAT-Luc), 300 ng of receptor, 1 to 200 ng of Gα subunit ($G\alpha_s$, 10 ng (for the $G\alpha_s$ titration 10 ng, 100 ng or 200 ng $G\alpha_s$ was used); $G\alpha_{olf}$, 100 ng; $G\alpha_i$, 100 ng; $G\alpha_q$, 200 ng; $G\alpha_{12}$, 1 ng; $G\alpha_{13}$, 10 ng; and PTX, 100 ng), and pcDNA5/FRT plasmid DNA to balance the total of DNA amount accordingly.

Twenty four hours posttransfection, the cells were washed with Dulbecco's PBS and detached in an enzyme-free solution. Cells were centrifuged for 3 min at 500 rcf, and the cell pellet was resuspended in 200 μl assay buffer (1 × HBSS, 20 mM Hepes, 0.1% wt/vol BSA, pH 7.5). Cells were distributed into a 96-well black/white IsoPlate (PerkinElmer Life Sciences) in triplicates at a volume of 60 μl/well. Finally, 30 μl of d-Luciferin dissolved in assay buffer was added to each well at a final concentration of 2 mM. After 30 min incubation, emission was read at 525 nm, using a PHERAstar FS microplate reader (BMG LABTECH). For assays using the SRE-Luc reporter, the medium was exchanged to serum-free DMEM 6 h after transfection.

50 μM forskolin-stimulated CRE reporter gene assays

HEK7GKO or HEK293T cells were seeded and transiently transfected as described for the Gα subunit screening, with 600 ng of CRE-Luc reporter, increasing amounts of the indicated receptor (10–600 ng), 160 ng $G\alpha_{s\Delta10}$ (for HEK7GKO cells only), and pcDNA5/FRT plasmid DNA to balance the DNA amount up to 1200 ng (1360 ng for the HEK7GKO cells). Twenty four hours posttransfection, the cells were detached and distributed into 96-well black/white IsoPlates, as described, before being stimulated with 10 μl forskolin per well to a final concentration of 50 μM for a total of 5 h. Thirty minutes before reading, d-Luciferin was added, and the plate was read as described above.

To ease the comparison of data between protocols, the receptor DNA (ng) in these experiments was scaled on the graphs to match the receptor plasmid DNA/cell ratio on the day of transfection. Data was presented as fold over the 0 ng receptor (600 ng empty vector) DNA point.

0 μM and 5 μM forskolin-stimulated CRE reporter gene assays

HEK293T, HEKΔGs, or HEK293A ("parental") cells were seeded at a density of 35,000 cells/well in PDL-coated, white 96-well microtiter plates and incubated overnight. Clear plates were prepared in parallel for ELISA. After 20 to 24 h, the media was aspirated, and the cells were transiently transfected directly in the wells using Lipofectamine2000 (0.6 μl/well) as follows (per well): 30 ng CRE-Luc reporter, cotransfected with increasing amounts of the indicated receptor or pcDNA3.1+ control (0–50 ng) in a total volume of 100 μl Opti-MEM. The total DNA amount was not balanced between the conditions. After 5 h, the transfection reaction was stopped with 100 μl/well growth media, and the cells were incubated overnight. Five hours before assay reading, the cells were supplemented with 5 μl/well forskolin or dimethylsulfoxid (vehicle) to a final concentration of 0 μM or 5 μM. Cells were washed with PBS^{++} and incubated with 100 μl of 1:1 dilution of SteadyLite:PBS^{++} for 30 min before emission was read at 400 to 700 nm using EnVision Multilabel microplate reader (PerkinElmer). Data were presented as fold over empty vector control curve (pcDNA3.1+ 0–50 ng DNA with or without 5 μM forskolin addition as indicated on the figure) for each data point.

PTX-cotransfected CRE reporter gene assays

Using the same transient transfection and assay protocol as above, HEK293T cells were transfected with (per well) 30 ng CRE-Luc reporter, 10 ng PTX-S1, 0 to 100 ng receptor, and pcDNA3.1+ to balance the DNA amount up to 140 ng. Data was presented as fold over the 0 ng receptor (100 ng empty vector) DNA point.

BRET assay (G-CASE, G-protein sensors)

ΔDVL1-3 cells were transiently transfected in suspension as described above, using 500 ng tricistronic $G\alpha_{i1/2/3}$ sensor and 500 ng of the indicated receptor or pcDNA3.1+ control, per 1 ml cell suspension. After 48 h incubation at growth conditions, the cells were washed with HBSS, and 100 μl/well of 10 μM Coelenterazine-H was added. After 10 min incubation, the nLuc (donor) emission was read at 480/30 nm, whereas cp-Venus (acceptor) emission was read at 535/30 nm, using EnVision Multilabel microplate reader (PerkinElmer). Six reads were recorded, and the mean of the three less varying serial reads was used to calculate the BRET ratio as emission [acceptor/donor].

Enzyme-linked immunosorbent assay

Transfected cells (see above) in clear 96-well microtiter plates were fixed in 100 μl, 3.7% formaldehyde in PBS++ for 10 min and washed twice in PBS^{++}. Cells were blocked in 2% BSA (w/v) in PBS^{++} for 30 min before being incubated with an anti-FlagM1 antibody (Sigma #F3040) diluted 1:2000 in 1% BSA (w/v) in PBS^{++} for 1 h. The cells were washed three times with PBS^{++} before incubation with goat anti-mouse-HRPconjugate IgG secondary antibody (Invitrogen #31430) diluted 1:1000 in 1% BSA (w/v) in PBS^{++} for 1 h. Next, the cells

were washed three times with PBS^{++} and incubated with 75 µl TMB PLUS2 (Kementec #4395A) for 0.5 to 3 min until the reaction was stopped with 0.2 M H_2SO_4. Absorbance was read at 450 nm using a FlexStation3 (Molecular Devices) microplate reader.

TCF/LEF luciferase reporter assay (TOPFlash)

Each ml cell suspension of $\Delta FZD_{1\text{-}10}$ HEK293T cells was transiently transfected with 500 ng pcDNA or receptor along with 100 ng pRL-TK_{Luc} (expression control) and 400 ng of M50 Super 8x TOPFlash (Addgene #12456). Cells grown in PDL-coated, white 96-well plates were washed with 120 ml HBSS/well 24 h posttransfection and incubated with FBS-free DMEM supplemented with 10 nM of the porcupine inhibitor C59 (Abcam# Ab142216). Four hours later, 1 µg/ml WNT3A or vehicle was added to the cells. Forty eight hours post-transfection, cells were washed with HBSS and lysed in 30 µl of Promega's dual luciferase passive lysis buffer (15 min at room temperature). Next, 20 µl luciferase assay reagent was added to each well, and reporter gene activity-dependent firefly luciferase intensity was measured using a CLARIOstar (580/80 nm; 1 s integration time) or Tecan Spark (585/70 nm; 2 s) microplate reader. Next, 20 µl Stop&Glo Reagent was added to quantify Renilla luciferase emission intensity (CLARIOstar: 480/80 nm; 1 s integration time; Tecan Spark: 487/85 nm; 2 s) to control for variations in cell number and transfection efficiency. Data were presented as firefly luciferase/Renilla luciferase intensity.

Statistical analysis

All data were analyzed using GraphPad Prism 9 (https://www.graphpad.com/). BRET ratio was calculated as emission [acceptor/donor]. One-way or two-way ANOVA using Tukey's *post hoc* test, or student's two-way, paired *t* test, was performed, as indicated in the Figure legends. Raw data was used for statistical analysis unless otherwise stated in the Figure legends. For all statistical tests, $p < 0.05$ was considered significant.

Data availability

All the data needed to evaluate the conclusions in the article are present in the paper or the Supplementary Materials.

Supporting information—This article contains supporting information.

Acknowledgments—We thank Nevin A. Lambert for the $G\alpha_{s\Delta 10}$ construct. We thank Asuka Ioue for the HEK7GKO and HEKΔGs cell lines, Benoit Vanhollebeke for the $\Delta FZD_{1\text{-}10}$ cell line, and Vítězslav Bryja for the ΔDVL1-3 cell line. We thank Maibritt S. Baggesen for technical support.

Author contributions—S. M. B., K. S., and M. M. R. conceptualization; S. M. B., H. S., A. L. S. W., A. K. D., T. P., C. K. K., M. M., and S. J. M. investigation; S. M. B., H. S., A.-S. M.-J., T. S., J. A. J., G. S., and K. S. methodology; S. M. B., and M. M. R. project administration; S. M. B. validation; S. M. B. writing–original draft; S. M. B., H. S., A. L. S. W., A. K. D., L. G., C. K. K., G. G. T., T. S., S. J. M., J. A. J., G. S., K. S., and M. M. R. writing–review and editing; S. M. B., H. S., A. K. D., C. K. K., S. J. M., and M. M. R. visualization; M. M. R. funding acquisition; M. M. R. supervision.

Funding and additional information—The research in the Rosenkilde laboratory was supported by the Novo Nordisk Foundation, NNF20OC0062899 (M. M. R.), the European Research Council (ERC) under the European Union's Horizon 2020 research and innovation programme, grant agreement No 682549 (M. M. R.), the Lundbeck Foundation, large project grant, R242-2017-409 (M. M. R.), a donation from deceased Valter Alex Torbjørn Eichmuller, 2020-117043 (M. M. R.) and Kirsten and Freddy Johansen's Foundation (KFJ), 2017-112697 (MMR). The work in the Schulte laboratory was supported by grants from Karolinska Institutet, the Swedish Research Council (2019-01190) (G. S.), the Swedish Cancer Society, 20 1102 PjF (G. S.), the Novo Nordisk Foundation NNF22OC0078104 (G. S.), The German Research Foundation (D. F. G.) project numbers 504098926 (L. G.); 427840891 (H. S.). Further work was supported by German Research Foundation (D. F. G.) CRC1423 project number 421152132 (T. S.), NIH grant MH54137 (J. A. J.), and NIH R35 grant GM149539 (G. G. T.). The content is solely the responsibility of the authors and does not necessarily represent the official views of the National Institutes of Health.

Conflict of interest—The authors declare that they have no conflicts of interest with the contents of this article.

Abbreviations—The abbreviations used are: aGPCR, adhesion G protein–coupled receptor; BRET, bioluminescence resonance energy transfer; BSA, bovine serum albumin; CRE, cAMP response element; CTF, C-terminal fragment; DMEM, Dulbecco's modified eagle medium; Dlg, discs large; DVL, disheveled; FBS, fetal bovine serum; FL, full length; FZD, frizzled; GPCR, G protein–coupled receptor; GPS, GPCR proteolytic site; HBSS, Hank's balanced salt solution; NFAT, nuclear factor of activated T cells; NFκB, nuclear factor κ-light-chain-enhancer of activated B cells; NTF, N-terminal fragment; PDL, poly-D lysine hydrobromide; PTX, pertussis toxin; SRE, serum response element; TCF/LEF, T-cell factor/lymphoid enhancer factor.

References

1. Schöneberg, T., and Liebscher, I. (2021) Mutations in G Protein–Coupled receptors: mechanisms, pathophysiology and potential therapeutic approaches. *Pharmacol. Rev.* **73**, 89–119
2. Langenhan, T. (2020) Adhesion G protein–coupled receptors—candidate metabotropic mechanosensors and novel drug targets. *Basic Clin. Pharmacol. Toxicol.* **126**, 5–16
3. Hamann, J., Aust, G., Arac, D., Engel, F. B., Formstone, C., Fredriksson, R., *et al.* (2015) International union of basic and clinical pharmacology. XCIV. Adhesion G protein-coupled receptors. *Pharmacol. Rev.* **67**, 338–367
4. Wittlake, A., Prömel, S., and Schöneberg, T. (2021) The evolutionary history of vertebrate adhesion GPCRs and its implication on their classification. *Int. J. Mol. Sci.* **22**, 11803
5. Bjarnadóttir, T. K., Fredriksson, R., Höglund, P. J., Gloriam, D. E., Lagerström, M. C., and Schiöth, H. B. (2004) The human and mouse repertoire of the adhesion family of G-protein-coupled receptors. *Genomics* **84**, 23–33
6. America, M., Bostaille, N., Eubelen, M., Martin, M., Stainier, D. Y. R., and Vanhollebeke, B. (2022) An integrated model for Gpr124 function in Wnt7a/b signaling among vertebrates. *Cell Rep.* **39**, 110902

7. Krasnova, O. A., Kulakova, K. A., Sopova, J. V., Smirnov, E. Y., Silonov, S. A., Lomert, E. V., *et al.* (2023) Essential role of adhesion GPCR, GPR123, for human pluripotent stem cells and reprogramming towards pluripotency. *Cells* **12**, 304
8. Lagerstrom, M. C., Rabe, N., Haitina, T., Kalnina, I., Hellstrom, A. R., Klovins, J., *et al.* (2007) The evolutionary history and tissue mapping of GPR123: specific CNS expression pattern predominantly in thalamic nuclei and regions containing large pyramidal cells. *J. Neurochem.* **100**, 1129–1142
9. Chang, J., Mancuso, M. R., Maier, C., Liang, X., Yuki, K., Yang, L., *et al.* (2017) Gpr124 is essential for blood–brain barrier integrity in central nervous system disease. *Nat. Med.* **23**, 450–460
10. Pickering, C., Hagglund, M., Szmydynger-Chodobska, J., Marques, F., Palha, J. A., Waller, L., *et al.* (2008) The Adhesion GPCR GPR125 is specifically expressed in the choroid plexus and is upregulated following brain injury. *BMC Neurosci.* **9**, 97
11. Li, X., Roszko, I., Sepich, D. S., Ni, M., Hamm, H. E., Marlow, F. L., *et al.* (2013) Gpr125 modulates Dishevelled distribution and planar cell polarity signaling. *Development* **140**, 3028–3039
12. Kvam, J. M., Nybo, M. L., Torz, L., Sustarsic, R. K., Jensen, K. H. R., Nielsen, J. E., *et al.* (2024) High incidence of imperforate vagina in ADGRA3-deficient mice. *BMC Biol.* **22**, 1–14
13. Spina, E., Simundza, J., Incassati, A., Chandramouli, A., Kugler, M. C., Lin, Z., *et al.* (2022) Gpr125 is a unifying hallmark of multiple mammary progenitors coupled to tumor latency. *Nat. Commun.* **13**, 1421
14. Fu, J.-F., Yen, T.-H., Chen, Y., Huang, Y.-J., Hsu, C.-L., Liang, D.-C., *et al.* (2013) Involvement of Gpr125 in the myeloid sarcoma formation induced by cooperating MLL/AF10(OM-LZ) and oncogenic KRAS in a mouse bone marrow transplantation model. *Int. J. Cancer* **133**, 1792–1802
15. Wu, Y., Chen, W., Gong, L., Ke, C., Wang, H., and Cai, Y. (2018) Elevated G-protein receptor 125 (GPR125) expression predicts good outcomes in colorectal cancer and inhibits wnt/β-catenin signaling pathway. *Med. Sci. Monitor* **24**, 6608–6616
16. Lei, P., Wang, H., Yu, L., Xu, C., Sun, H., Lyu, Y., *et al.* (2022) A correlation study of adhesion G protein-coupled receptors as potential therapeutic targets in Uterine Corpus Endometrial cancer. *Int. Immunopharmacol.* **108**, 108743
17. Seandel, M., James, D., Shmelkov, S. V., Falciatori, I., Kim, J., Chavala, S., *et al.* (2007) Generation of functional multipotent adult stem cells from GPR125+ germline progenitors. *Nature* **449**, 346
18. Nybo, M. L., Kvam, J. M., Nielsen, J. E., Frederiksen, H., Spiess, K., Jensen, K. H. R., *et al.* (2023) Loss of Adgra3 causes obstructive azoospermia with high penetrance in male mice. *FASEB J.* **37**, e22781
19. [preprint] Spina, E., Handlin, R., Simundza, J., Incassati, A., Faiq, M., Sainulabdeen, A., *et al.* (2020) Gpr125 identifies myoepithelial progenitors at tips of lacrimal ducts and is essential for tear film. *bioRxiv*. https://doi.org/10.1101/2020.09.15.296749
20. Zhao, Z., Hu, L., Song, B., Jiang, T., Wu, Q., Lin, J., *et al.* (2024) Constitutively active receptor ADGRA3 signaling induces adipose thermogenesis. *Elife* **13**, RP100205
21. Sakurai, T., Kamakura, S., Hayase, J., Kohda, A., Nakamura, M., and Sumimoto, H. (2022) GPR125 (ADGRA3) is an autocleavable adhesion GPCR that traffics with Dlg1 to the basolateral membrane and regulates epithelial apicobasal polarity. *J. Biol. Chem.* **298**, 102475
22. Knapp, B., Roedig, J., Boldt, K., Krzysko, J., Horn, N., Ueffing, M., *et al.* (2019) Affinity proteomics identifies novel functional modules related to adhesion GPCRs. *Ann. N. Y Acad. Sci.* **1456**, 144–167
23. Yamamoto, Y., Irie, K., Asada, M., Mino, A., Mandai, K., and Takai, Y. (2004) Direct binding of the human homologue of the Drosophila disc large tumor suppressor gene to seven-pass transmembrane proteins, tumor endothelial marker 5 (TEM5), and a novel TEM5-like protein. *Oncogene* **23**, 3889–3897
24. Tang, C.-Y., Wang, H., Zhang, Y., Wang, Z., Zhu, G., McVicar, A., *et al.* (2022) GPR125 positively regulates osteoclastogenesis potentially through AKT-NF-κB and MAPK signaling pathways. *Int. J. Biol. Sci.* **18**, 2392–2405
25. Arac, D., Boucard, A. A., Bolliger, M. F., Nguyen, J., Soltis, S. M., Sudhof, T. C., *et al.* (2012) A novel evolutionarily conserved domain of cell-adhesion GPCRs mediates autoproteolysis. *EMBO J.* **31**, 1364–1378
26. Krasnoperov, V., Lu, Y., Buryanovsky, L., Neubert, T. A., Ichtchenko, K., and Petrenko, A. G. (2002) Post-translational proteolytic processing of the calcium-independent receptor of alpha-latrotoxin (CIRL), a natural chimera of the cell adhesion protein and the G protein-coupled receptor. Role of the G protein-coupled receptor proteolysis site (GPS) moti. *J. Biol. Chem.* **277**, 46518–46526
27. Paavola, K. J., Stephenson, J. R., Ritter, S. L., Alter, S. P., and Hall, R. A. (2011) The N terminus of the adhesion G protein-coupled receptor GPR56 controls receptor signaling activity. *J. Biol. Chem.* **286**, 28914–28921
28. Dates, A. N., Jones, D. T. D., Smith, J. S., Skiba, M. A., Rich, M. F., Burruss, M. M., *et al.* (2024) Heterogeneity of tethered agonist signaling in adhesion G protein-coupled receptors. *Cell Chem. Biol.* **31**, 1542–1553.e4
29. Stoveken, H. M., Hajduczok, A. G., Xu, L., and Tall, G. G. (2015) Adhesion G protein-coupled receptors are activated by exposure of a cryptic tethered agonist. *Proc. Natl. Acad. Sci. U. S. A.* **112**, 6194–6199
30. Liebscher, I., Schön, J., Petersen, S. C., Fischer, L., Auerbach, N., Demberg, L. M., *et al.* (2014) A tethered agonist within the ectodomain activates the adhesion G protein-coupled receptors GPR126 and GPR133. *Cell Rep.* **9**, 2018–2026
31. Kleinau, G., Ali, A. H., Wiechert, F., Szczepek, M., Schmidt, A., Spahn, C. M. T., *et al.* (2023) Intramolecular activity regulation of adhesion GPCRs in light of recent structural and evolutionary information. *Pharmacol. Res.* **197**, 106971
32. Knierim, A. B., Röthe, J., Çakir, M. V., Lede, V., Wilde, C., Liebscher, I., *et al.* (2019) Genetic basis of functional variability in adhesion G protein-coupled receptors. *Sci. Rep.* **9**, 11036
33. Kuhn, C. K., Stenzel, U., Berndt, S., Liebscher, I., Schöneberg, T., and Horn, S. (2024) The repertoire and structure of adhesion GPCR transcript variants assembled from publicly available deep-sequenced human samples. *Nucleic. Acids Res.* **52**, 3823–3836
34. Paclíková, P., Radaszkiewicz, T. W., Potěšil, D., Harnoš, J., Zdráhal, Z., and Bryja, V. (2021) Roles of individual human dishevelled paralogs in the Wnt signalling pathways. *Cell Signal.* **85**, 110058
35. Bjarnadóttir, T. K., Geirardsdóttir, K., Ingemansson, M., Mirza, M. A. I., Fredriksson, R., and Schiöth, H. B. (2007) Identification of novel splice variants of Adhesion G protein-coupled receptors. *Gene* **387**, 38–48
36. Salzman, G. S., Ackerman, S. D., Ding, C., Koide, A., Leon, K., Luo, R., *et al.* (2016) Structural basis for regulation of GPR56/ADGRG1 by its alternatively spliced extracellular domains. *Neuron* **91**, 1292–1304
37. Boucard, A. A., Maxeiner, S., and Südhof, T. C. (2014) Latrophilins function as heterophilic cell-adhesion molecules by binding to teneurins: regulation by alternative splicing. *J. Biol. Chem.* **289**, 387–402
38. Aust, G., Hamann, J., Schilling, N., and Wobus, M. (2003) Detection of alternatively spliced EMR2 mRNAs in colorectal tumor cell lines but rare expression of the molecule in colorectal adenocarcinomas. *Virchows Archiv.* **443**, 32–37
39. Lorenzi, L., Chiu, H. S., Avila Cobos, F., Gross, S., Volders, P. J., Cannoodt, R., *et al.* (2021) The RNA Atlas expands the catalog of human non-coding RNAs. *Nat. Biotechnol.* **39**, 1453–1465
40. Kawamura, S., Matsushita, Y., Kurosaki, S., Tange, M., Fujiwara, N., Hayata, Y., *et al.* (2022) Inhibiting SCAP/SREBP exacerbates liver injury and carcinogenesis in murine nonalcoholic steatohepatitis. *J. Clin. Invest.* **132**, e151895
41. Pantazatos, S. P., Huang, Y. Y., Rosoklija, G. B., Dwork, A. J., Arango, V., and Mann, J. J. (2017) Whole-transcriptome brain expression and exon-usage profiling in major depression and suicide: evidence for altered glial, endothelial and ATPase activity. *Mol. Psychiatry.* **22**, 760–773
42. Okashah, N., Wan, Q., Ghosh, S., Sandhu, M., Inoue, A., Vaidehi, N., *et al.* (2019) Variable G protein determinants of GPCR coupling selectivity. *Proc. Natl. Acad. Sci. U. S. A.* **116**, 12054–12059

43. Martin, A. L., Steurer, M. A., and Aronstam, R. S. (2015) Constitutive activity among orphan class-A G protein coupled receptors. *PLoS One* **10**, e0138463
44. Mathiasen, S., Palmisano, T., Perry, N. A., Stoveken, H. M., Vizurraga, A., McEwen, D. P., *et al.* (2020) G12/13 is activated by acute tethered agonist exposure in the adhesion GPCR ADGRL3. *Nat. Chem. Biol.* **16**, 1343–1350
45. McLean, K. A., Holst, P. J., Martini, L., Schwartz, T. W., and Rosenkilde, M. M. (2004) Similar activation of signal transduction pathways by the herpesvirus-encoded chemokine receptors US28 and ORF74. *Virology* **325**, 241–251
46. Faas, F., Nørskov, A., Holst, P. J., Andersson, A.-M., Qvortrup, K., Mathiasen, S., *et al.* (2023) Re-routing GPR56 signalling using Gα12/13 G protein chimeras. *Basic Clin. Pharmacol. Toxicol.* **133**, 378–389
47. Mavri, M., Kubale, V., Depledge, D. P., Zuo, J., Huang, C. A., Breuer, J., *et al.* (2022) Epstein-barr virus-encoded BILF1 orthologues from porcine lymphotropic herpesviruses display common molecular functionality. *Front. Endocrinol. (Lausanne)* **13**, 862940
48. Paulsen, S. J., Rosenkilde, M. M., Eugen-Olsen, J., and Kledal, T. N. (2005) Epstein-barr virus-encoded BILF1 is a constitutively active G protein-coupled receptor. *J. Virol.* **79**, 536–546
49. Stallaert, W., Van Der Westhuizen, E. T., Schönegge, A. M., Plouffe, B., Hogue, M., Lukashova, V., *et al.* (2017) Purinergic receptor transactivation by the β2-adrenergic receptor increases intracellular Ca2+ in nonexcitable cells. *Mol. Pharmacol.* **91**, 533–544
50. Hansen, H. S., Rosenkilde, M. M., Holst, J. J., and Schwartz, T. W. (2012) GPR119 as a fat sensor. *Trends Pharmacol. Sci.* **33**, 374–381
51. Hassing, H. A., Fares, S., Larsen, O., Pad, H., Hauge, M., Jones, R. M., *et al.* (2016) Biased signaling of lipids and allosteric actions of synthetic molecules for GPR119. *Biochem. Pharmacol.* **119**, 66–75
52. Katada, T., Tamura, M., and Ui, M. (1983) The A protomer of islet-activating protein, pertussis toxin, as an active peptide catalyzing ADP-ribosylation of a membrane protein. *Arch. Biochem. Biophys.* **224**, 290–298
53. Schihada, H., Shekhani, R., and Schulte, G. (2021) Quantitative assessment of constitutive G protein–coupled receptor activity with BRET-based G protein biosensors. *Sci. Signal.* **14**, 1653
54. Schihada, H., Klompstra, T. M., Humphrys, L. J., Cervenka, I., Dadvar, S., Kolb, P., *et al.* (2022) Isoforms of GPR35 have distinct extracellular N-termini that allosterically modify receptor-transducer coupling and mediate intracellular pathway bias. *J. Biol. Chem.* **298**, 102328
55. Eubelen, M., Bostaille, N., Cabochette, P., Gauquier, A., Tebabi, P., Dumitru, A. C., *et al.* (2018) A molecular mechanism for Wnt ligand-specific signaling. *Science* **361**, eaat1178
56. Hu, Q. X., Dong, J. H., Du, H. B., Zhang, D. L., Ren, H. Z., Ma, M. L., *et al.* (2014) Constitutive Gαi coupling activity of very large G protein-coupled receptor 1 (VLGR1) and its regulation by PDZD7 protein. *J. Biol. Chem.* **289**, 24215–24225
57. Shin, D., Lin, S. T., Fu, Y. H., and Ptácek, L. J. (2013) Very large G protein-coupled receptor 1 regulates myelin-associated glycoprotein via Gαs/Gαq-mediated protein kinases A/C. *Proc. Natl. Acad. Sci. U. S. A.* **110**, 19101–19106
58. Rahman, M. A., Ashton, A. C., Meunier, F. A., Davletov, B. A., Dolly, J. O., and Ushkaryov, Y. A. (1999) Norepinephrine exocytosis stimulated by latrotoxin requires both external and stored Ca2 and is mediated by latrophilin, G proteins and phospholipase C. *Philos. Trans. R Soc. Lond B Biol. Sci.* **354**, 379–386
59. Müller, A., Winkler, J., Fiedler, F., Sastradihardja, T., Binder, C., Schnabel, R., *et al.* (2015) Oriented cell division in the C. elegans embryo is coordinated by G-protein signaling dependent on the adhesion GPCR LAT-1. *PLoS Genet.* **11**, e1005624
60. Petersen, S. C., Luo, R., Liebscher, I., Giera, S., Jeong, S. J., Mogha, A., *et al.* (2015) The adhesion GPCR GPR126 has distinct, domain-dependent functions in schwann cell development mediated by interaction with laminin-211. *Neuron* **85**, 755–769
61. Daaka, Y., Luttrell, L. M., and Lefkowitz, R. J. (1997) Switching of the coupling of the beta2-adrenergic receptor to different G proteins by protein kinase A. *Nature* **390**, 88–91
62. Xiao, R. P., Ji, X., and Lakatta, E. G. (1995) Functional coupling of the beta 2-adrenoceptor to a pertussis toxin-sensitive G protein in cardiac myocytes. *Mol. Pharmacol.* **47**, 322–329
63. Xiao, P., Guo, S., Wen, X., He, Q. T., Lin, H., Huang, S. M., *et al.* (2022) Tethered peptide activation mechanism of the adhesion GPCRs ADGRG2 and ADGRG4. *Nat.* **604**, 771–778
64. Ping, Y. Q., Xiao, P., Yang, F., Zhao, R. J., Guo, S. C., Yan, X., *et al.* (2022) Structural basis for the tethered peptide activation of adhesion GPCRs. *Nat.* **604**, 763–770
65. Qu, X., Qiu, N., Wang, M., Zhang, B., Du, J., Zhong, Z., *et al.* (2022) Structural basis of tethered agonism of the adhesion GPCRs ADGRD1 and ADGRF1. *Nat.* **604**, 779–785
66. Barros-Álvarez, X., Nwokonko, R. M., Vizurraga, A., Matzov, D., He, F., Papasergi-Scott, M. M., *et al.* (2022) The tethered peptide activation mechanism of adhesion GPCRs. *Nat.* **604**, 757–762
67. Spiess, K., Bagger, S. O., Torz, L. J., Jensen, K. H. R., Walser, A. L., Kvam, J. M., *et al.* (2019) Arrestin-independent constitutive endocytosis of GPR125/ADGRA3. In **, 1456**. *Annals of the New York Academy of Sciences*, Blackwell Publishing Inc.: 186–199
68. Cho, C., Smallwood, P. M., and Nathans, J. (2017) Reck and Gpr124 are essential receptor cofactors for Wnt7a/Wnt7b-specific signaling in mammalian CNS angiogenesis and blood-brain barrier regulation. *Neuron* **95**, 1056–1073.e5
69. Bostaille, N., Gauquier, A., Twyffels, L., and Vanhollebeke, B. (2016) Molecular insights into Adgra2/Gpr124 and Reck intracellular trafficking. *Biol. Open* **5**, 1874–1881
70. Vanhollebeke, B., Stone, O. A., Bostaille, N., Cho, C., Zhou, Y., Maquet, E., *et al.* (2015) Tip cell-specific requirement for an atypical Gpr124- and Reck-dependent Wnt/β-catenin pathway during brain angiogenesis. *Elife* **4**, 1–25
71. Cho, C., Wang, Y., Smallwood, P. M., Williams, J., and Nathans, J. (2019) Molecular determinants in Frizzled, Reck, and Wnt7a for ligand-specific signaling in neurovascular development. *Elife* **8**, e47300
72. Vallon, M., Yuki, K., Nguyen, T. D., Chang, J., Yuan, J., Siepe, D., *et al.* (2018) A RECK-WNT7 receptor-ligand interaction enables isoform-specific regulation of wnt bioavailability. *Cell Rep.* **25**, 339–349.e9
73. Berndt, J. D., Aoyagi, A., Yang, P., Anastas, J. N., Tang, L., and Moon, R. T. (2011) Mindbomb 1, an E3 ubiquitin ligase, forms a complex with RYK to activate Wnt/β-catenin signaling. *J. Cell Biol.* **194**, 737–750
74. Green, J., Nusse, R., and van Amerongen, R. (2014) The role of Ryk and Ror receptor tyrosine kinases in wnt signal transduction. *Cold Spring Harb. Perspect. Biol.* **6**, a009175
75. Lin, S., Baye, L. M., Westfall, T. A., and Slusarski, D. C. (2010) Wnt5b-Ryk pathway provides directional signals to regulate gastrulation movement. *J. Cell Biol.* **190**, 263–279
76. Bowin, C.-F., Inoue, A., and Schulte, G. (2019) WNT-3A-induced β-catenin signaling does not require signaling through heterotrimeric G proteins. *J. Biol. Chem.* **294**, 11677–11684
77. Hilbig, D., Dietrich, N., Wandel, E., Gonsior, S., Sittig, D., Hamann, J., *et al.* (2018) The interaction of CD97/ADGRE5 with β-catenin in adherens junctions is lost during colorectal carcinogenesis. *Front. Oncol.* **8**, 182
78. Shashidhar, S., Lorente, G., Nagavarapu, U., Nelson, A., Kuo, J., Cummins, J., *et al.* (2005) GPR56 is a GPCR that is overexpressed in gliomas and functions in tumor cell adhesion. *Oncogene* **24**, 1673–1682
79. He, L., Arnold, C., Thoma, J., Rohde, C., Kholmatov, M., Garg, S., *et al.* (2022) CDK7/12/13 inhibition targets an oscillating leukemia stem cell network and synergizes with venetoclax in acute myeloid leukemia. *EMBO Mol. Med.* **14**, e14990
80. Dobin, A., and Gingeras, T. R. (2016) Optimizing RNA-seq mapping with STAR. *Methods Mol. Biol.* **1415**, 245–262

81. Li, H., Handsaker, B., Wysoker, A., Fennell, T., Ruan, J., Homer, N., *et al.* (2009) The sequence alignment/map format and SAMtools. *Bioinformatics* **25**, 2078–2079
82. Pertea, M., Pertea, G. M., Antonescu, C. M., Chang, T. C., Mendell, J. T., and Salzberg, S. L. (2015) StringTie enables improved reconstruction of a transcriptome from RNA-seq reads. *Nat. Biotechnol.* **33**, 290–295
83. Cock, P. J. A., Antao, T., Chang, J. T., Chapman, B. A., Cox, C. J., Dalke, A., *et al.* (2009) Biopython: freely available Python tools for computational molecular biology and bioinformatics. *Bioinformatics* **25**, 1422–1423
84. Paysan-Lafosse, T., Blum, M., Chuguransky, S., Grego, T., Pinto, B. L., Salazar, G. A., *et al.* (2023) InterPro in 2022. *Nucleic Acids Res.* **51**, D418–D427
85. Lord, S. J., Velle, K. B., Dyche Mullins, R., and Fritz-Laylin, L. K. (2020) SuperPlots: communicating reproducibility and variability in cell biology. *J. Cell Biol.* **219**, e202001064